The Journal of Young Investigators
The premier undergraduate research journal

Computer Generation of Three Dimensional Human Cerebral Vasculature Models

Shinita Thomas and Smit Naik
University of Illinois at Chicago

Volume 19, Issue 17
November 2009

Computer Generation of Three Dimensional Human Cerebral Vasculature Models

Shinita Thomas and Smit Naik
University of Illinois at Chicago
Correspondence: sthoma42@uic.edu

Mentor: Dr. Andreas A. Linninger
Advisor: Brian Sweetman

Abstract
Recent clinical findings suggest changes in vasculature compliance may be responsible for abnormal brain dynamics in diseases like hydrocephalus. Understanding and treating pathological brain dynamics requires a quantitative understanding of the complex interaction between pulsating vasculature, cerebrospinal fluid, and brain tissue. Models addressing anatomically correct geometry, physiological haemodynamics and complete interactions of vasculature and brain tissue are required for this purpose. In this article, a geometrical model of the cerebral vasculature is presented as a first step in the development of a fully distributed mathematical model for quantitative analysis of intracranial dynamics. We present two- and three- dimensional models of the human cerebral vasculature network. The model was generated in two phases. First, the major extracerebral arteries were reconstructed using patient-specific MRI images. Then in step two a special modified algorithm of Beard & Bassingthwaighte generated the microvasculature, starting from the major arteries of step one. This fractal-based growth algorithm incorporates vessel and complex domain boundary avoidance to create the vasculature. Significant findings are: (1) MRI imaging was successful in generating patient specific geometry of the brain cerebral arteries including carotid artery, basilar artery, Circle of Willis and vertebral arteries; (2) a microvasculature below the medical imaging resolution was successfully created by the computer algorithm; (3) vessels consistently remained inside the domain boundary and avoided overlap; (4) model capillary density agrees qualitatively with actual human capillary density. However, there were some limitations to the model. The model is not completely consistent with the cerebral vasculature anatomy due to limited MRI resolution and the absence of physiological driving forces for the vessel growth in the algorithm. Future work will focus on acquiring quantitatively accurate capillary density in the model by incorporating growth factors in the algorithm. Work is being done toward incorporating blood vessel branching factors and constrained optimization techniques into the algorithm. Moreover, in the next step blood flow simulations need to be performed to predict blood flow and vessel dilations.

Introduction

In humans, a pair of internal carotid arteries and vertebral arteries delivers 15-20% of the cardiac output to the brain (Mokhtar, 2007). These arteries branch and join together to form the Circle of Willis, an arterial system that ensures uninterrupted blood flow in case of pressure variations in the brain. Downstream, deoxygenated blood is drained out of the brain by the venous system made up of exterior and interior cerebral veins. Small capillaries in the brain connect the arteries with veins and complete the blood network of the brain. Capillaries together with arterioles and venules form the microvasculature as shown in Figure 1.

Cerebral blood flow aids transportation of hormones and removal of metabolic wastes. Moreover, blood supplies oxygen and glucose to nerve cells of the brain which control various functions of the body. Pulsatile blood flow effects the movement of cerebrospinal fluid (CSF), a clear, plasma-like fluid of the brain that acts as a shock absorbing cushion and assists homeostasis

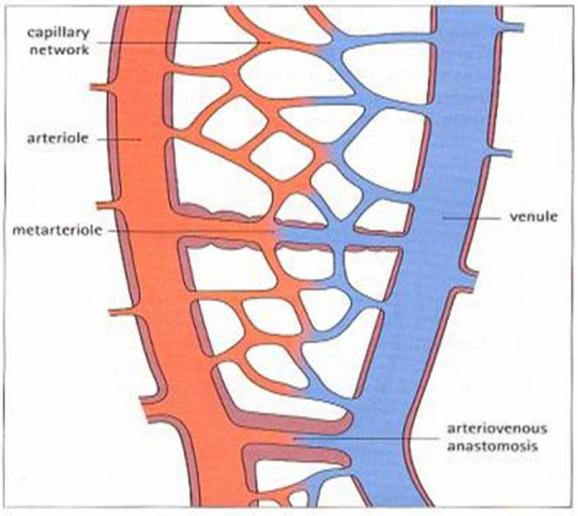

Figure 1. General model of microvasculature showing arterioles connected to venules via capillary system (Stevens & Lowe, 2005).

and metabolism in the brain. According to Bhadelia, et al. (1997) the pulsatile blood flow causes a bi-directional oscillatory movement of the cerebrospinal fluid. Because blood vessels are elastic, they expand and contract in response to changes in blood pressure throughout the cardiac cycle. This expansion causes CSF from the subarachnoid space to be displaced from the cranium into the spinal canal. The displacement of CSF into the spinal canal is necessary due to the volume consistency of the cranium and is possible due to the distensibility of the lower lumbar region of the spinal canal (Jirout, 1967). Microvasculature expansion also causes brain tissue strain leading to compression of the lateral ventricles and outflow of CSF from the ventricular system. On average, the total capillary expansion is about 0.03 ml and matches the ventricular CSF stroke volume (Greitz, 2004).

Modeling cerebral blood flow will provide valuable insight into the complex interactions between expanding vasculature, displaceable CSF, and deformable brain tissue. Through modeling, we aim to predict physiologically accurate blood flow rates and pressure distribution throughout the cerebral vasculature network. A careful analysis of cerebral blood flow mechanics will further lead to greater understanding about vascular diseases such as arteriosclerosis, atherosclerosis, arterio-venous malformation, and even tumor growth (Baish, Netti, & Jain, 1997; Gabriel & Yang, 2007; Kassianos, 2008). Furthermore, a cerebral blood flow model may help to elucidate the underlying pathophysiology of normal pressure hydrocephalus (NPH). NPH is a disease of the central nervous system whose pathophysiology has been hypothesized to be vascular in origin (Greitz, 2004).

Many *compartmental* (or lumped) models of cerebral vasculature have been proposed over the last few decades. The mathematical model proposed by Zagzoule and Marc-Vergnest in 1986 was one of the first models accounting for the effects of microvasculature resistance to the overall blood flow dynamics (1986). Their model assumes blood to be incompressible and viscous and reduces the microvasculature to a single vessel, reducing the complexity of modeling and analysis. Recently, *distributed* cerebral vasculature models have been proposed (Beard & Bassingthwaighte, 2000; Bui, Sutalo, Manasseh, & Liffman, 2009; Karch, Neumann, Neumann, & Schreiner, 1999; Schreiner, 1993; Schreiner, et al., 2006). In a distributed cerebral vasculature model the vessels would be modeled as they exist in nature. Modeling vasculature in this way (as opposed to lumped models) may provide greater insight into how brain tissue, cerebral vasculature, and CSF interact. Using a distributed model one could predict local stresses near the cerebral ventricles (Linninger, Sweetman, & Penn, 2009). Also the volume change of the cerebrum over the course of the cardiac cycle could be studied in greater detail. It has been reported that vasculature expansion is greater in the hydrocephalic brain compared to normal subjects (Greitz, 2004). This larger expansion could mean that in hydrocephalic patients, brain water content changes are significantly higher over the course of the cardiac cycle as compared to normal subjects. This is a question requiring more study and whose implications are still unknown. Nevertheless, a distributed model of the brain and cerebral vasculature is necessary to answer questions such as this.

To our knowledge, a fully distributed model of the entire cerebral vasculature including arteries, arterioles, capillaries, venules, and veins has not been developed. This is due in large part to limitations of current imaging and manual segmentation techniques. Currently, no method exists to reconstruct the microvasculature for computational modeling. Many approaches use fractals or *fractal-like* concepts to produce microvasculature (Bui, et al., 2009; Marxen & Henkelman, 2003). Constrained Constructive Optimization (CCO) proposed by Schreiner is used to construct large arteries in complex domains (Schreiner, 1993; Schreiner & Buxbaum, 1993; Schreiner, et al., 2006). The CCO algorithm produces realistic networks for arteries but seems to be limited in generating microvasculature. In this report we describe a new method for reconstructing the vasculature network. This model will generate
new insights about the blood flow dynamics and cerebral vascular diseases. Extracerebral arteries were reconstructed from patient-specific computer tomography (CT) scans using manual segmentation. Microvasculature was generated using vessel-avoidance and boundary-avoidance algorithms. The algorithms generate new vessels by avoiding the domain boundary and previously generated vessels.

The paper is organized as follows: The methods section describes the algorithm for constructing the microvasculature. The results section will show the completed vasculature model. The article concludes with a discussion of results, strengths and shortcomings of the current approach, and presents our plans for future work in vasculature modeling.

Materials and Methods

Brain boundary and arterial reconstruction

To begin the process of building a human brain vasculature model, the brain boundary was reconstructed from 120 axial CT images using

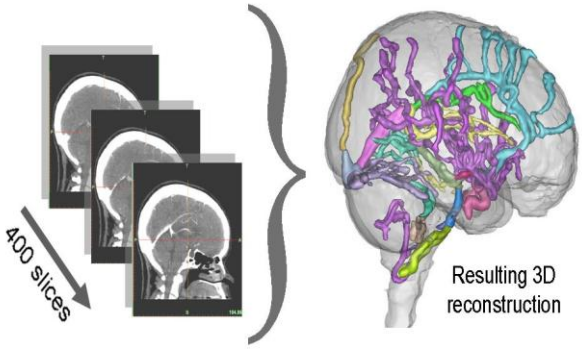

Figure 2. CT angiography images were used to reconstruct main human arteries and veins. The vessel thickness is magnified for better visibility.

manual segmentation (Materialise, Belgium). The resulting surface mesh served as the vasculature domain. Next, 400 CT brain images were used to reconstruct the extracerebral arteries as shown in Figure 2. The location and connectivity of the extracerebral arteries were used as input to reconstruct the microvasculature inside the brain boundary.

Self-avoidance and boundary- avoidance algorithms

An algorithm first devised by Beard and Bassingthwaighte (2000) was modified to generate microvasculature inside the geometrically complex brain domain. In the algorithm, vasculature is broken down into elements and segments. The first element is assigned the order 1 and the branches have orders 2 to 11, the larger vessels having lowest orders. Furthermore, each element is composed of a specified number of segments that provide realistic shape and flexibility to the vessels. Two constraints that account for true vasculature phenomena were incorporated into the algorithm. First, new vessels should not intersect or overlap previously generated vessels. Second, vessels should not go beyond the brain boundary. These two constraints required a *self-avoidance* algorithm and a *boundary-avoidance* algorithm (Beard & Bassingthwaighte, 2000).

The self-avoidance algorithm restricts new vessels from growing toward regions of established vessels. This algorithm provides an *intermediate* direction for the new vessel. Each existing vessel segment repels new vascular growth away from its position with a strength inversely related to the distance between its endpoint and the origin of the new vessel as in eq. ((1). Thus, new vessels will grow toward sparse regions of the domain.

Self-avoidance algorithm

$$\vec{v}_s = \sum_i \frac{(L_s/d_i)^\zeta}{1+(L_s/d_i)^\zeta} \cdot \hat{y}_i = \sum_i strength(i) \cdot \hat{y}_i \qquad (1)$$

In eq. ((1), L_s is the segment length, d_i is the distance from x_u to x_i, ζ is the avoidance exponent that controls the spread and branching of vessels ($\zeta = 3$ is found to be the best and is used in the models), and $\hat{y}_i$ is the unit vector from x_u to x_i. x_u is the starting point of the vessel to be generated and x_i represents all previously generated points.

The boundary-avoidance algorithm calculates the *final* direction of the new segment influenced by the direction of the intermediate vector and all points on the domain boundary. The algorithm, governed by eq. ((2), forces vessels to avoid points on the boundary, so that vessels are generated only within the domain.

Boundary-avoidance algorithm

$$\hat{d} = \frac{\underset{\sim}{v}_s + \sum_{j=1}^{N_B} \hat{n}_j e^{-d_j/2L_s}}{\left| \underset{\sim}{v}_s + \sum_{j=1}^{N_B} \hat{n}_j e^{-d_j/2L_s} \right|} \qquad (2)$$

In eq. ((2) $\hat{d}$ is the final direction of the new vessel segment, $\underset{\sim}{v}_s$ is the unit vector of $\vec{v}_s$, calculated in eq. ((1), N_B is the number of boundary points, d_j is the distance between boundary point j and x_u, and L_s is the new vessel length. $\hat{n}_j$ is a unit vector directed from each boundary point toward x_u; $\hat{n}_j$ repels new vessel segments away from the boundary. Incorporating

the influence of established vessels and boundary points the new point can be calculated as follows:

$$x_d = x_u + L_s \hat{d} \quad (3)$$

In eq. (3) x_d is the new point, i.e., the terminal point of the new vessel, x_u is the new vessel's origin, $\hat{d}$ is the final direction, and L_s the length of the segment. A conceptual diagram

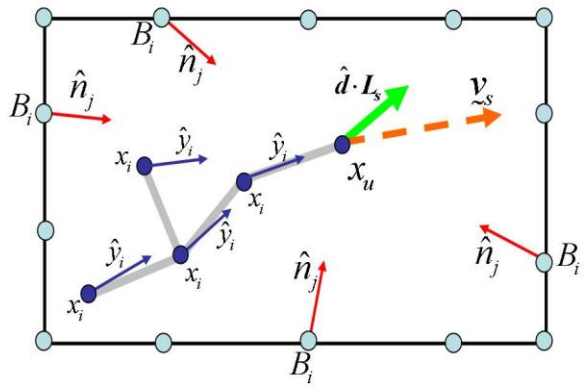

Figure 5. Diagram showing how the new vessel direction is calculated. Orange, dashed vector represents the preliminary vessel direction calculated by the self-avoidance algorithm. Green vector represents the final direction calculated by the boundary-avoidance algorithm.

showing the intermediate vessel and final new vessel is given in Figure 3.

Results

Two-dimensional vascular generation

To ensure the code was working properly, initially, vessels were generated in a mid-sagittal cross section of a human brain. Vessels were found to avoid the domain boundary as well as previously generated vessels. Figure 4 shows a small network of 95 branches. Although rather simple, the model does help to visualize the penetration of large vessels into the brain tissue. The red vessels penetrating into the tissue bifurcate into smaller arterioles and capillaries. Downstream arterioles (blue) and capillaries (green) avoid overlap, consistent with the vessel-avoidance algorithm constraint.

Vascular generation in three-dimensional brain boundary

The cerebral vasculature model is shown in Figure 5. The brain boundary is oriented from anterior (left) to posterior (right) in the figure. Each arteriole (red) in frame (a) contributes 100 branches to the capillary bed (blue). The inset shows details of the vasculature and displays vessel density. In the model, the number of branches and segments were increased to more closely match experimental measurements of brain capillary

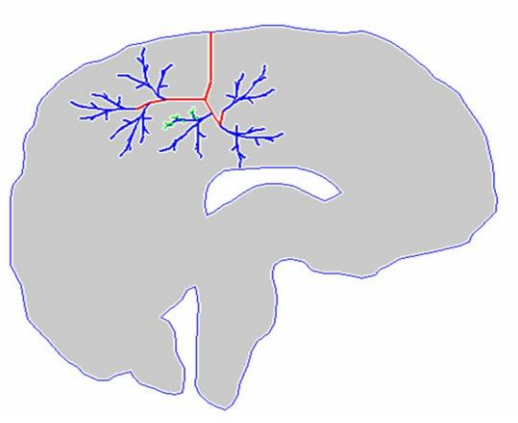

Figure 4. Two-dimensional vessel-avoidance and boundary-avoidance algorithm in a mid-sagittal cross section of a human brain. Proof of concept that the algorithm works in a complex domain.

density (Anderson, Tan, & Meyer, 1999). This progression in model detail is shown in frames (b) and (c) in which each arteriole produces 200 and 400 branches, respectively. Furthermore, the length of the segments was reduced drastically at the level of the smaller vessels to provide a realistic appearance. More capillaries are found in the interior of the human brain and less on the surface. Special weights

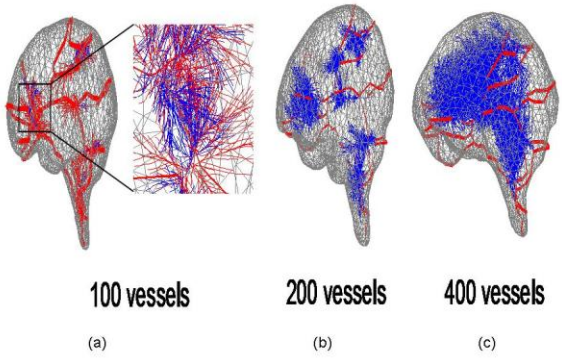

Figure 3. Three images of vasculature with major extracerebral arteries. Eight major arterioles penetrate into the tissue and form capillaries. (a) Each arteriole contributes 100 branches for the capillary bed. (b) Each arteriole forms 200 branches and longer segments. (c) Each arteriole forms 400 longer branches and fills the brain.

were added to the $\hat{n}_j$ vector in the boundary avoidance algorithm to attain this density. The thickness of the lines was varied to represent the difference in diameters of different types of vessels; arteries being thicker and capillaries being the thinnest.

Discussion

Our three-dimensional cerebral vasculature model incorporates arteries and microvasculature inside a human brain. The vascular domain was created from a set of medical images using manual segmentation techniques. Specially designed algorithms were implemented in Matlab to produce the microvasculature bed. A vessel-avoidance algorithm caused new vessels to avoid previously generated vessels, and a boundary-avoidance algorithm guided the vasculature growth inside the domain boundary. To improve the effectiveness of the boundary-avoidance algorithm, the vasculature domain was made up of 38,682 points. Increasing the number of boundary points increased the repulsive effect, and vessels consistently remained inside the domain. Moreover, $\hat{n}_j$ was scalar-weighted to more effectively drive vessels into the domain.

Model predictions of capillary density

Human capillary diameter is 7-10 μm and the intercapillary distance is about 54.90-60.52 μm. Capillary density in the human adult brain on average is 338 capillaries/mm^2 (600 capillaries/mm^3) (Anderson, et al., 1999; Freitas, 1999). The model results of capillary density with actual data from human micrographs are found to be qualitatively similar. Research suggests capillary density is greater in grey matter than in white matter (Cavaglia, et al., 2001; Niemineva & Tervila, 1953). This fact may be due to the presence of more cell bodies and synapses in the grey matter. Neuronal somas have a high metabolic rate and require high levels of oxygen and nutrients which are delivered by capillaries. Higher capillary density in grey matter has been incorporated into the final model by growing more capillaries toward the walls of the boundary and less toward the center. This step will need refinement in future models since white and grey regions are interwoven. Delineating their boundaries requires more advanced manual segmentation.

In future studies we propose one of two methods to ensure the model contains actual capillary density (338 capillaries/mm^2). One method is to incorporate into our algorithm a concept from the fractal literature, namely, fractal dimension. Fractal dimension is a mathematical entity that defines the branching of fractals from higher to lower orders. Fractal dimension incorporates space filling effects associated with artery and microvasculature branching. Another possibility for matching the capillary density is to include *pseudo growth factors* in our design algorithm. For instance, evidence supports the idea that specific growth factors influence angiogenesis (Jones & Sleeman, 2006). It may be possible to guide the capillaries into certain regions of the brain domain, having them branch in such a way to meet the constraints of the growth factors. This concept needs to be investigated further; work by Nekka (Nekka, Kyriacos, Kerrigan, & Cartilier, 1996) could be used as a starting point. Furthermore, the blood volume through each vessel could be geometrically optimized using optimization techniques similar to the Constrained Constructive Optimization (Schreiner, 1993; Schreiner & Buxbaum, 1993; Schreiner, et al., 2006). Incorporating any of these methods may lead to a capillary density and branching factor that is similar to actual human data. However, these approaches were beyond the scope of this investigation and will be accomplished in the future research. Nevertheless, using only the vessel avoidance and the boundary avoidance algorithms a similar capillary density was attained in the model.

Vasculature visualization and blood flow simulation

The current network is composed of the major arteries, arterioles, and capillaries. A venous system comprising major veins and venules still needs to be generated and added to the final model to complete the vasculature network. At this point, however, the capillary network will be sufficient to study changes in brain pulsation in a blood flow model of the human brain. Blood flow simulations were beyond the scope of this study and will be the focus of future work. Blood flow through the vasculature network can be achieved with a quasi-transient cardiac pressure input signal. Elastic vasculature walls that pulsate with changes in lumen pressure assumption will help to obtain realistic flow values.

In the model, differences in vessel lumen diameter were visualized by varying the thickness of lines; thicker lines were assigned to arteries and thinner lines for arterioles and capillaries. This step does not influence the final outcome of the vasculature generation and merely serves as a

visualization tool. When blood flow is simulated through the network, the vessel radii will be of great importance and will be a specific parameter in the equations of fluid flow.

Conclusion

In this report the reconstruction of extracerebral arteries from medical images and microvasculature generation using specially designed algorithms are described. A human brain and major extracerebral arteries were reconstructed from medical images. These major arteries were used as input to generate arterioles and capillaries. Self-avoidance and boundary-avoidance algorithms generated a detailed capillary network; the capillary density generated in the model is in good agreement with actual human micrograph data. However, the model has some limitations because the growth of vessels is only driven by geometric optimization. Physiological conditions of controlling the growth of vessels is absent in the model. Incorporating criteria like fractal dimension, *pseudo growth factors* or constrained optimization techniques will help to improve the branching of vessels. Nevertheless, the present work is a preliminary step toward completing a fully distributed model of the human central nervous system. Such a model would be helpful in studying the complex interactions between distensible cerebral vasculature, deformable brain tissue, and CSF flow.

Acknowledgments

The authors would like to thank Dr. Andreas A. Linninger and Brian J. Sweetman for the guidance and support throughout the project. Shinita Thomas and Smit Naik are also grateful to all members of Laboratory for Product and Process Design, University of Illinois at Chicago. We acknowledge Ms. Nabiha Shamsi, who performed the initial work on the extracerebral vasculature reconstruction. Shinita Thomas is grateful for the funding from Research for Undergraduate Experience stipend under the National Science Foundation grant, NSF EEC 0754590 entitled Novel Processes and Materials in Bioengineering and Biomedical Engineering (A. Linninger, PI).

References

Anderson, R. E., Tan, W. K., & Meyer, F. B. (1999) Brain acidosis, cerebral blood flow, capillary bed density, and mitochondrial function in the ischemic penumbra. J Stroke Cerebrovasc Dis 8(6), 368-379.

Baish, J. W., Netti, P. A., & Jain, R. K. (1997) Transmural coupling of fluid flow in microcirculatory network and interstitium in tumors. Microvasc Res 53(2), 128-141.

Beard, D. A., & Bassingthwaighte, J. B. (2000) The fractal nature of myocardial blood flow emerges from a whole-organ model of arterial network. J Vasc Res 37(4), 282-296.

Bhadelia, R. A., Bogdan, A. R., Kaplan, R. F., & Wolpert, S. M. (1997) Cerebrospinal fluid pulsation amplitude and its quantitative relationship to cerebral blood flow pulsations: a phase-contrast MR flow imaging study. Neuroradiology 39(4), 258-264.

Blood Vasculature Network. (2008). from http://www.bordalierinstitute.com/images/bloodVascularNetwork.jpg

Bui, A., Sutalo, I. D., Manasseh, R., & Liffman, K. (2009) Dynamics of pulsatile flow in fractal models of vascular branching networks. Med Biol Eng Comput 47(7), 763-772.

Cavaglia, M., Dombrowski, S. M., Drazba, J., Vasanji, A., Bokesch, P. M., & Janigro, D. (2001) Regional variation in brain capillary density and vascular response to ischemia. Brain Res 910(1-2), 81-93.

Freitas, R. A. (1999). Nanomedicine. from http://www.foresight.org/Nanomedicine/

Gabriel, R. A., & Yang, G. Y. (2007) Gene therapy in cerebrovascular diseases. Curr Gene Ther 7(6), 421-433.

Greitz, D. (2004) Radiological assessment of hydrocephalus: new theories and implications for therapy. Neurosurg Rev 27(3), 145-165; discussion 166-147.

Jirout, J. (1967) Dynamics of the spinal dural sac under normal conditions. Br J Radiol 40(471), 209-213.

Jones, P. F., & Sleeman, B. D. (2006) Angiogenesis - understanding the mathematical challenge. Angiogenesis 9(3), 127-138.

Karch, R., Neumann, F., Neumann, M., & Schreiner, W. (1999) A three-dimensional model for arterial tree representation, generated by

constrained constructive optimization. Comput Biol Med 29(1), 19-38.

Kassianos, G. (2008) New insights into atherothrombotic disease. Primary Health Care 18(6), 39-39.

Linninger, A. A., Sweetman, B., & Penn, R. (2009) Normal and hydrocephalic brain dynamics: the role of reduced cerebrospinal fluid reabsorption in ventricular enlargement. Ann Biomed Eng 37(7), 1434-1447.

Marxen, M., & Henkelman, R. M. (2003) Branching tree model with fractal vascular resistance explains fractal perfusion heterogeneity. Am J Physiol Heart Circ Physiol 284(5), H1848-1857.

Mokhtar, Y. (2007). Cerebral Circulation. from http://www.doctorslounge.com/studlounge/articles/cerebcirc/cerebcirc1.htm

Nekka, F., Kyriacos, S., Kerrigan, C., & Cartilier, L. (1996) A model of growing vascular structures. Bull Math Biol 58(3), 409-424.

Niemineva, K., & Tervila, L. (1953) On the capillary bed of the human fetal cerebellar hemispheres. Acta Anat (Basel) 19(3), 204-209.

Ponkshe, S., Linninger, A. A., Xenos, M., & Zhang, L. (2008) Computer Modeling of Physiological Conditions for Better Understanding of Intracranial Blood Pressure and Brain Vasculature. Journal of Young Investigators 19.

Schreiner, W. (1993) Computer generation of complex arterial tree models. J Biomed Eng 15(2), 148-150.

Schreiner, W., & Buxbaum, P. F. (1993) Computer-optimization of vascular trees. IEEE Trans Biomed Eng 40(5), 482-491.

Schreiner, W., Karch, R., Neumann, M., Neumann, F., Szawlowski, P., & Roedler, S. (2006) Optimized arterial trees supplying hollow organs. Med Eng Phys 28(5), 416-429.

Stevens, A., & Lowe, J. S. (2005). *Human histology* (3rd ed.). Philadelphia ;: Elsevier/Mosby ;.

Zagzoule, M., & Marc-Vergnes, J. P. (1986) A global mathematical model of the cerebral circulation in man. J Biomech 19(12), 1015-1022.